Plume-ridge interaction induced migration of the Hawaiian-Emperor seamounts

Wei-Dong Sun, Charles H Langmuir, Neil M. Ribe, Li-Peng Zhang, Sai-Jun Sun, He Li, Cong-Ying Li, Wei-Ming Fan, Paul J Tackley, Patrick Sanan

Plume-ridge interaction induced migration of the Hawaiian-Emperor plume

Wei-dong Sun[1-3]*, Charles H. Langmuir[4]*, Neil M. Ribe[5], Li-peng Zhang[1,3], Sai-jun Sun[1,3], He Li[1,2], Cong-ying Li[1,2], Wei-ming Fan[3,6], Paul J. Tackley[7] and Patrick Sanan[7]

[1] Center of Deep Sea Research, Center of Ocean Mega Science, Institute of Oceanology, Chinese Academy of Sciences, Qingdao 266071, China

[2] Laboratory for Marine Mineral Resources, Pilot National Laboratory for Marine Science and Technology (Qingdao), Qingdao 266237, China

[3] University of the Chinese Academy of Sciences, Beijing 100049, China

[4] Department of Earth and Planetary Sciences, Harvard University, Cambridge, USA.

[5] Univ Paris 11, CNRS, Lab FAST, F-91405 Orsay, France

[6] CAS Center for Excellence in Tibetan Plateau Earth Sciences, Chinese Academy of Sciences, Beijing 100101, China

[7] Institute of Geophysics, Department of Earth Sciences, ETH Zurich, Sonneggstrasse 5, 8092 Zűrich, Switzerland*

*Corresponding authors: Wei-dong Sun; Charles H. Langmuir.

Email: weidongsun@qdio.ac.cn; langmuir@eps.harvard.edu

Abstract

The history of the Hawaiian hotspot is of enduring interest in studies of plate motion and mantle flow, and has been investigated by many using the detailed history of the Emperor Seamount chain. One of the unexplained aspects of this history is the apparent offset of several Emperor seamounts from the Hawaii plume track. Here we show that the volcanic migration rates of the Emperor seamounts based on existing data are inconsistent with the drifting rate of the Pacific plate, and indicate northward and then southward absolute movements of the Hawaiian plume. Numerical modeling suggests that attraction and capture of the plume by a moving spreading ridge led to variation in the location of the plume's magmatic output at the surface. Flow of the plume material towards the ridge led to apparent southward movement of Meiji. Then, the plume was carried northward between 76 and 65 Myr ago. After ridge and plume became sufficiently separated, magmatic output rapidly moved back to be centered over the plume between 61 and 50 Myr. These changes are apparent in variations in volume along the plume track. Chemical and isotopic compositions of basalt from the Emperor Seamount chain changed from depleted (strong mid-ocean ridge affinity) in Meiji and Detroit to enriched (ocean island type), supporting declining influence from a spreading center. Although its surface expression was modified by mantle flow and by plume-ridge interactions, the stem of the Hawaiian plume may have been essentially stationary during the Emperor period.

Keywords

Pacific plate; Emperor-Hawaii chain; plume-ridge interaction; geochemistry; numerical modeling

Main Text

The Emperor-Hawaiian volcanic chain consists of ~130 volcanoes and stretches for more than 6000 km across the Pacific plate. It played a key role in supporting the theory of plate tectonics and the plume hypothesis that suggested the Hawaiian-Emperor chains formed by a moving Pacific plate coupled with a stationary mantle plume [1, 2]. The famous bend between the Emperor and

the Hawaiian chains has been attributed to a major change in the drifting direction of the Pacific plate [1-4]. This has been challenged by paleomagnetic results, however, which suggest that the Detroit seamount (76-82 Myr) erupted at a paleolatitude of ~36°N. The surface expression of the plume then moved southward towards the current latitude (19°N) [5, 6]. Consequently, it has been proposed that the Emperor Seamount trend formed by the rapid migration of the Hawaiian plume between 81 to 47.5 Myr ago, instead of changes in the direction of the Pacific plate [5], although this conclusion is by no means universally accepted [3, 7]. Any explanation for the tracking of the Emperor Seamounts prior to the bend must take into account the clear correlation between distance and age revealed by dating of the volcanoes of the Hawaiian chain. One of the features of this relationship, however, is that between about 80 and 55 Myr, the linear relationship breaks down (Figure 1e) with offsets from the linear trend of as much as 300 km relative to the stationary Louisville seamount chain [8]. The offset has previously been explained by a combination of hotspot and plate motion changes driven by plate/mantle reorganization [8]. Others have proposed that the misfit between different reconstructions related to the Hawaiian-Emperor chains was due to intraplate deformation [9], whereas the paleomagnetic data were partially due to true polar wander [4].

Here we show that the volcanic migration rate of the Emperor seamounts calculated from ages [3] and distance between corresponding seamounts differ from the drifting rate of the Pacific plate obtained through plate reconstruction based on magnetic anomalies using GPlates [10] (Figure 1). This discrepancy seems to require first a northward (Detroit to Suiko) and then a southward (Suiko to Koko) movement of the Hawaiian plume. When these movements are viewed in the context of the changes in the volume of the Emperor Seamount chain with time, and the variations in the geochemistry of the erupted volcanic rocks, they suggest that interaction of the plume with the spreading center that were in the north Pacific at that time may be the cause of the age-distance disparities (Figure 1a-e).

High precision ages together with relative distances for volcanoes of the Emperor Seamount chain can be used to calculate the changes in migration rate between ~ 76 to 50 Myr ago [3]. Based on isotopic dating results [3], the fast migration of the volcanos from Suiko to Nintoku (8.9 $\pm$ 1.4 cm/year) and then to Koko (17 $\pm$ 5.4 cm/year) occurred between 60.9 $\pm$ 0.3 and 52.6 $\pm$ 0.8 Myr. In contrast, according to plate reconstruction, the Pacific plate drifted slowly (~ 2.9 to 5.4 cm/year) during this period. This misfit requires rapid southward migration of the surface expression of the hot spot by 670 ± 280 km. In contrast, at older times the migration rate of the Hawaiian plume based on volcano ages is smaller than the drifting rate of the Pacific plate between ~76 and 60.9 Myr, obtained using the same methods, which requires northward migration of the plume by 610 ± 230 km, consistent with the distance of the southward migration within error (Figure 1d).

During these time periods, the volume of the Emperor Seamount chain also changed progressively. This is readily apparent from the map view of the seamount chain (Figure 1c), but surface volumes are quantified in Figure 1a. The volumes are the greatest for the oldest parts of the seamount chain, Detroit and Meiji seamounts. They decrease and then stabilize at about half the maximum volume, until they decrease to low values between Nintoku and Ojin (See the map in Fig. 1c).

These observations then suggest an explanation for the time-distance relationships of the Emperor seamounts that were influenced by plume-ridge interaction. Interactions between spreading ridges and mantle plumes are common in the Earth's history [11-16] and have previously been proposed as an explanation for the Hawaii-Emperor bend (7). As shown by numerical modeling (Figure 2 and Supplementary Information), as a spreading ridge moves, the interacting mantle plume may be deflected/carried along for millions of years through entrainment of plume flow by the ridge [17-20]. The interaction may also change the migration rate of the ridge [11], e.g., leading to ridge jump towards the plume, forming asymmetric sea-floor spreading [21, 22]. Jellinek et al point out that plume is attracted towards an approaching ridge and eventually captured by it, leading to a surface manifestation of volcanism that is offset relative to the deep plume stem [23].

Our numerical modeling suggests that as the moving ridge approaches the plume, the plume is attracted towards the ridge, leading to an apparent offset in the plume position (Figure 2). Deeply rooted plume magmas can then be preferentially channeled to and erupted at the ridge-axis with increased melt production. As the ridge subsequently moves away from the plume, the plume is no longer deflected and volcanism moves rapidly back to be positioned over the deeply rooted plume stem (Figure 2).

Schilling identified this tendency long ago by adopting the term “plume source-ridge sink”, when he showed that plumes far off-axis could be focusing some of their material to ridges several hundred kilometer distant [24]. Jellinek et al point out that faster spreading ridges can be particularly effective in entraining plume flow [23]. Previous numerical modeling consistently suggests that the plume may be offset by several hundred kilometers [20]. Wessel and Kroenke discussed the potential effects of plume-ridge interaction in the Emperor chain to explain the relative motion of Hawaii and Louisville plumes. They, however, thought “it remains a speculative scenario that is difficult to test” [4]. Our modeling clearly indicates that plume-ridge interaction may plausibly explain the offsets obtained by comparing the migration of the Emperor seamounts and the drifting of the Pacific plate.

These various considerations of volume, geochemistry, observations of plume capture by spreading centers elsewhere and theoretical models raise the possibility that plume-ridge interaction influenced the ancient plume that formed the Emperor Seamounts. At the time of formation of the oldest part of the chain, the Hawaiian plume first encountered the approaching ridge, leading to a slight southward movement of the shallow part of the plume to feed the ridge. This led to increases in volume and a depleted chemical signature of basalts as the ridge approached the plume. As the ridge moved northwards away from the plume, plume flow remained entrained by the ridge, distorting the age-distance relationships. Once the ridge was far enough away, plume flow would become vertical once again, causing a rapid migration of surface volcanism. The rapid migration would lead to low volumes at the surface until the surface volcanism

was once again stably aligned over the deep plume center. This would account for the low volumes of the Emperor chain, apparent in the map and volume data, between Nintoku and Ojin seamounts (Figure 1 a-c).

The geochemical signatures of basalts from the Emperor Seamount chain also change systematically with time from depleted (similar to mid-ocean ridge basalt, MORB like) to enriched (ocean island basalt, OIB, affinities) [25, 26], with significant correlations between ages (or distance) and isotope and element ratios (Figure 3). For example, the average $^{87}Sr/^{86}Sr$ increases from a MORB value of 0.70275 in Detroit volcanic rocks up to an OIB value of 0.70357 in Mauna Kea basalts (Figure 3a). The change in average Nd isotope composition is less striking. It drops from $^{143}Nd/^{144}Nd = 0.51312$ (in the range of MORB values) to $^{143}Nd/^{144}Nd = 0.513029$ in Ojin basalts (similar to those of Mauna Kea) (Figure 3b). The average $^{3}He/^{4}He$ ratio increases with decreasing ages, from 10.6 ± 1.95 (close to MORB values) in Detroit volcano to typical OIB values of 21.35 ± 1.90 in Koko samples (Figure 3c) [26]. Trace element ratios sensitive to MORB and OIB components also correlate with age. The average La/Yb ratios increase from MORB values of 0.96 ± 0.01 in Detroit volcano to typical OIB values of 13.75 ± 9.16 in Koko samples (Figure 3d). The average Zr/Y ratios increase from 2.49 ± 0.03 in Detroit to 9.66 ± 2.61 in Koko (Figure 3e). These geochemical characteristics can be plausibly explained by mixing of enriched and depleted components (Supplementary Figure S6 and Dataset S2).

The MORB affinities of the Emperor volcanos increased from Meiji at ~ 85 Myr and peaked at Detroit at 76-82 Myr and then declined continuously (Figure 3). The MORB affinities of the Meiji basalt suggest the commencement of the ridge-plume interaction with southward migration at ~85 Myr, which may also have been responsible for the gap between Bowers and Shirshov Ridges. In addition, the Meiji and Detroit seamounts are similar to oceanic plateaus in size, much larger than other Emperor Seamounts. There is also a relationship between the estimated volumes of the individual Emperor Seamounts and the proportions of depleted components in the sampled basalts (Figure 3f).

Plume magmas form through decompression partial melting of hot mantle materials. The thickness of oceanic lithosphere decreases towards the spreading ridge. When a plume is beneath the ridge, the upwelling distance of plume materials is considerably increased, and the plume is diluted by normal asthenospheric mantle, as well as undergoing larger degrees of partial melting. Consequently, in addition to enriched components (OIB affinities), depleted (MORB-like) components that are refractory under normal oceanic lithosphere, are also melted [25].

Viewed from this perspective, both the volume and geochemical data suggest that the ancient Hawaiian plume was interacting with a spreading center. At ~85 Myr, the plume was attracted southward to a spreading center (to 19° N, Supplementary Figure S7), leading to large eruptive volumes and more depleted compositions. This is consistent with plate reconstructions using GPlates and previous results [4, 11, 27], which suggest that the Hawaiian plume was near the northern Pacific spreading centers at ~85 Myr.

The Detroit volcano has ages ranging from 82-76 Myr, with large fluctuations in paleolatitude (~26-40°N) [5]. This cannot be explained by migration of the plume, because Meiji is right next to Detroit. Note, Meiji was erupted at ~19°N 82-85 Myr ago, the same as current Hawaii (Supplementary Figure S7) [28], which is consistent with the stationary mantle plume model [2]. Our results show that the upper part of the Hawaiian plume was carried northward between Detroit and Suiko, with an offset of ~ 600 km (Figure 1d and 2). This can plausibly explain the paleolatitudes of Detroit within error. In addition, there might be a true polar wander during this period [4].

In this case Meiji seamounts were erupted when the plume was drawn southward into the ridge. The southward movement of the plume may have started at the Bowers Ridges in the Bering Sea [27], which explains the gap between the Bowers and the Shirshov Ridges. As the spreading ridge moved to the north, plume volcanism was shifted towards it, forming Detroit, Suiko etc. As the ridge moved further, it lost contact with the Hawaiian plume, leading to the exceptionally rapid southern migration as plume magmatism returned to the top of the plume stem (Figure 4).

Ridge-plume interaction at Detroit has long been identified by geochemists [25]. Previous studies have proposed that the Hawaiian plume may have been captured by a moving ridge [6]. However, the authors then argued that the plume was further carried by sub-Pacific mantle flow [6], and that “the Hawaiian-Emperor chain bend morphology was caused by hotspot motion, not plate motion” [29]. The plume-mantle interaction model was taken as “a speculative scenario that is difficult to test” [4].

Such ridge-plume interactions are supported by plate reconstructions. The spreading ridge between the Izanagi and the Pacific plates moved northward at least since 125 Ma and passed over the Hawaiian plume. Plate reconstruction shows that the Hawaiian plume may have started to interact with the Pacific-Izanagi spreading ridge at ~ 90 Myr ago [11]. Our results suggest that the stem of the Hawaiian plume likely had a stable location from 47.5 to 85 Myr. The discrepancies with the linear age-distance trends were caused by the interaction of the plume with the spreading ridge during this period. This would resolve the problem of very fast migration rates, and the discrepancies between the Hawaiian and Louisville hot spot tracks, and account for the marked changes in eruption volumes and chemical compositions during this time period.

Conflict of Interest

The authors declare no competing interests.

Acknowledgments

This study was supported by MOST of China 2016YFC0600408, CAS XDB18020000, to W.D.S. N.M.R. acknowledges support from grant BFC 221950 from the Progamme National de Planétologie (PNP) of the Institut des Sciences de l'Univers (INSU) of the CNRS. We thank Professor A.W. Hofmann for constructive discussions.

Author Contributions

W.D.S. initiated the study, conceived and drafted the manuscript. L.P.Z. carried plate reconstruction using GPlates and plotted related figures. C.H.L. provided key points and suggestions on the chemical characteristics and volume of the seamounts that dramatically improved the manuscript. N.M.R. did the numerical modeling. S.J.S. plotted the geochemical figures. P.J.T. and P. S. wrote and maintained the code StagYY. W.D.S. and C.H.L. finalized the manuscript with input from all authors.

References

[1] Wilson JT. A possible origin of hawaiian islands. Can J Phys 1963; 41: 863-&

[2] Morgan WJ. Deep mantle convection plumes and plate motions. American Association of Petroleum Geologists Bulletin 1972; 56: 203-&

[3] Sharp WD, Clague DA. 50-ma initiation of hawaiian-emperor bend records major change in pacific plate motion. Science 2006; 313: 1281-1284

[4] Wessel P, Kroenke LW. Observations of geometry and ages constrain relative motion of hawaii and louisville plumes. Earth Planet Sci Lett 2009; 284: 467-472

[5] Tarduno JA, Duncan RA, Scholl DW, et al. The emperor seamounts: Southward motion of the hawaiian hotspot plume in earth's mantle. Science 2003; 301: 1064-1069

[6] Tarduno J, Bunge H-P, Sleep N, et al. The bent hawaiian-emperor hotspot track: Inheriting the mantle wind. Science 2009; 324: 50-53

[7] Torsvik TH, Doubrovine PV, Steinberger B, et al. Pacific plate motion change caused the hawaiian-emperor bend. Nat Commun 2017; 8: 12

[8] O'Connor JM, Steinberger B, Regelous M, et al. Constraints on past plate and mantle motion from new ages for the hawaiian-emperor seamount chain. Geochemistry Geophysics Geosystems 2013; 14: 4564-4584

[9] Steinberger B, Sutherland R, O'Connell RJ. Prediction of emperor-hawaii seamount locations from

a revised model of global plate motion and mantle flow. Nature 2004; 430: 167-173

[10] Seton M, Muller RD, Zahirovic S, et al. Global continental and ocean basin reconstructions since 200 ma. Earth-Sci Rev 2012; 113: 212-270

[11] Whittaker JM, Afonso JC, Masterton S, et al. Long-term interaction between mid-ocean ridges and mantle plumes. Nature Geoscience 2015; 8: 479-U484

[12] Ribe NM. The dynamics of plume-ridge interaction .2. Off-ridge plumes. Journal of Geophysical Research-Solid Earth 1996; 101: 16195-16204

[13] Walters RL, Jones SM, Maclennan J. Renewed melting at the abandoned hunafloi rift, northern iceland, caused by plume pulsing. Earth Planet Sci Lett 2013; 377: 227-238

[14] Kincaid C, Ito G, Gable C. Laboratory investigation of the interaction of off-axis mantle plumes and spreading centres. Nature 1995; 376: 758-761

[15] Webber AP, Roberts S, Taylor RN, et al. Golden plumes: Substantial gold enrichment of oceanic crust during ridge-plume interaction. Geology 2013; 41: 87-90

[16] Stroncik NA, Devey CW. Recycled gabbro signature in hotspot magmas unveiled by plume-ridge interactions. Nature Geoscience 2011; 4: 393-397

[17] Georgen JE. Interaction of a mantle plume and a segmented mid-ocean ridge: Results from numerical modeling. Earth Planet Sci Lett 2014; 392: 113-120

[18] Geldmacher J, Hoefig TW, Hauff F, et al. Influence of the galapagos hotspot on the east pacific rise during miocene superfast spreading. Geology 2013; 41: 183-186

[19] Small C. Observations of ridge-hotspot interactions in the southern ocean. Journal of Geophysical Research: Solid Earth 1995; 100: 17931-17946

[20] Sleep NH. Lateral flow of hot plume material ponded at sublithospheric depths. Journal of Geophysical Research: Solid Earth 1996; 101: 28065-28083

[21] Muller RD, Roest WR, Royer JY. Asymmetric sea-floor spreading caused by ridge-plume interactions. Nature 1998; 396: 455-459

[22] Mittelstaedt E, Soule S, Harpp K, et al. Multiple expressions of plume-ridge interaction in the

galapagos: Volcanic lineaments and ridge jumps. Geochemistry Geophysics Geosystems 2012; 13: 31

[23] Jellinek AM, Gonnermann HM, Richards MA. Plume capture by divergent plate motions: Implications for the distribution of hotspots, geochemistry of mid-ocean ridge basalts, and estimates of the heat flux at the core-mantle boundary. Earth Planet Sci Lett 2003; 205: 361-378

[24] Schilling J-G. Fluxes and excess temperatures of mantle plumes inferred from their interaction with migrating mid-ocean ridges. Nature 1991; 352: 397-403

[25] Regelous M, Hofmann AW, Abouchami W, et al. Geochemistry of lavas from the emperor seamounts, and the geochemical evolution of hawaiian magmatism from 85 to 42 ma. J Petrol 2003; 44: 113-140

[26] Keller RA, Graham DW, Farley KA, et al. Cretaceous-to-recent record of elevated he-3/he-4 along the hawaiian-emperor volcanic chain. Geochemistry Geophysics Geosystems 2004; 5: 10

[27] Steinberger B, Gaina C. Plate-tectonic reconstructions predict part of the hawaiian hotspot track to be preserved in the bering sea. Geology 2007; 35: 407-410

[28] Marshall M. The magnetic properties of some dsdp basalts from the north pacific and inferences for pacific plate tectonics. Journal of Geophysical Research: Solid Earth 1978; 83: 289-308

[29] Bono RK, Tarduno JA, Bunge HP. Hotspot motion caused the hawaiian-emperor bend and llsvps are not fixed. Nat Commun 2019; 10: 9

Figures

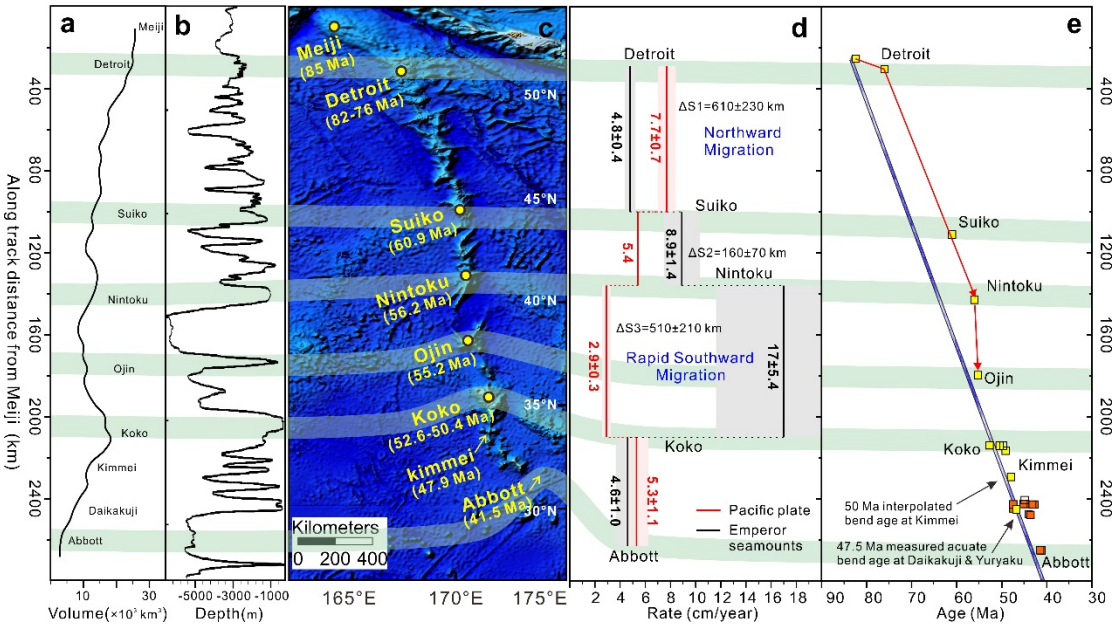

Figure 1. Along track profiles of volume and depth, migration rate of the Pacific plate and Emperor seamounts, and relative positions of Emperor seamounts and Louisville seamounts. a, Along track volume profile (five-point running average) of the Emperor Seamount chain, showing low volume between Nintoku and Ojin. The high volumes associated with Koko may be owing to a fossil ridge. **b,** Along track depth profile of the Emperor Seamount chain, which also shows the lowest depths between Nintoku and Ojin. **c,** Map showing the positions and ages of Emperor seamounts. Note there is no seamount between Nintoku and Ojin. Base map is from NOAA (https://www.ngdc.noaa.gov/). **d,** The northward migration rate of the Emperor seamounts based on high precision ages [3] and the northward migration rate of the Pacific plate calculated from plate reconstruction using GPlates [10] (averaged between seamounts). The different migration rates suggest that the Hawaiian plume moved northward relative to the mantle framework before ~ 61 Myr (Suiko), and then changed to southward absolute motions. **e,** Age-distance diagram modified after reference [8], showing two major offsets, which corresponds to a northward migration near Detroit seamount and a rapid southward migration between Nintoku and Ojin. All these support plume-ride interaction: the plume was captured by a northward migrating ridge and migrated northward; it then migrated southward rapidly once the ridge lost control on the plume.

Both the volume and the depth profiles were obtained using ArcGIS and bathymetry data (GEBCO, https://www.gebco.net/).

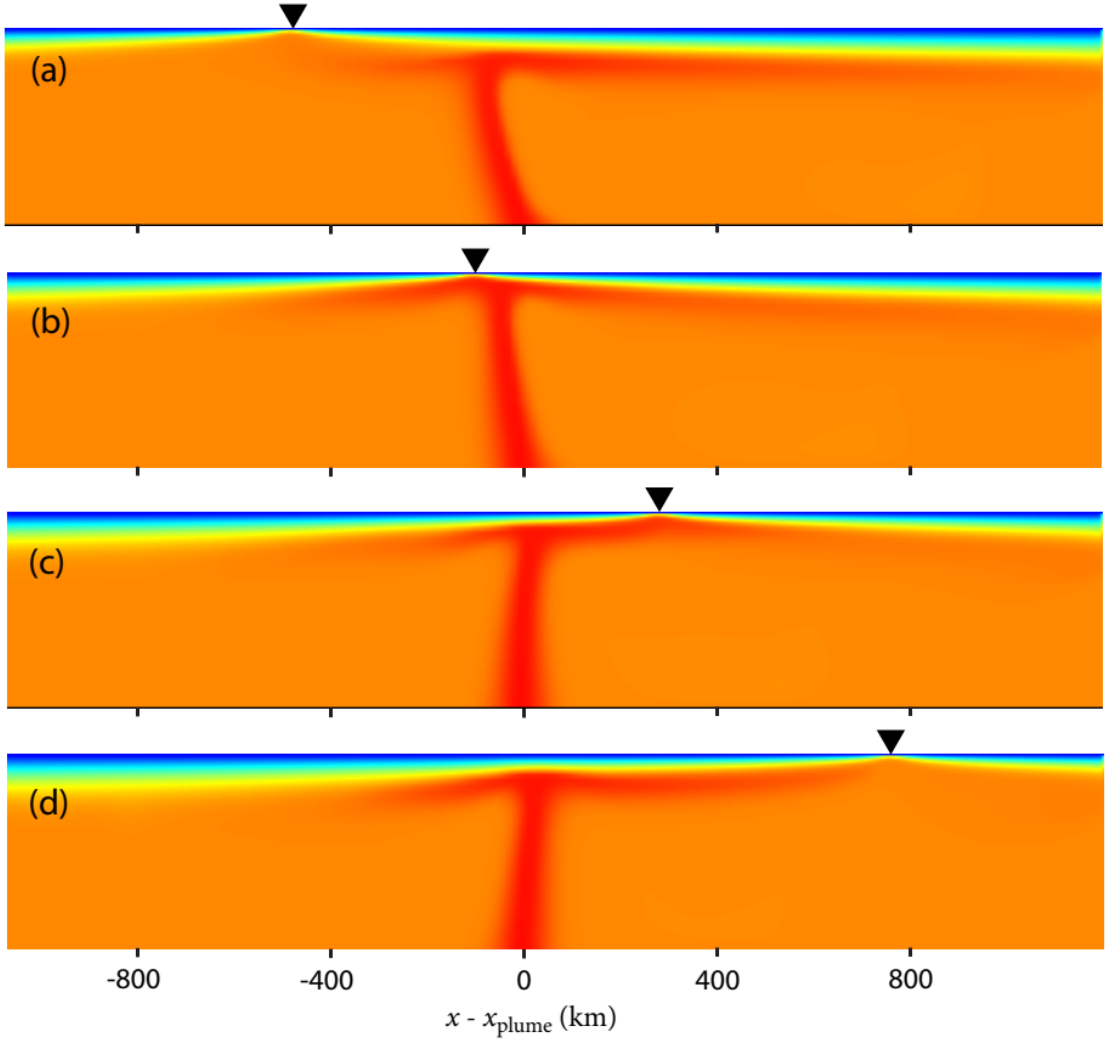

Figure 2. Typical evolution of plume-ridge interaction predicted by the numerical model. The plume has radius a = 55 km and excess temperature ΔT = 250 K, and the half-spreading rate and migration rate of the ridge are U = Um = 3.2 cm/yr. The mantle plume is attracted towards the ridge at a distance of ~ 580 kilometers, and then carried by the moving ridge. The melting is intensified dramatically during this process. The ridge lost control on the plume when it is ~ 620 kilometers away from the original position of the plume stem. Please refer to the Supplementary materials for more detailed information.

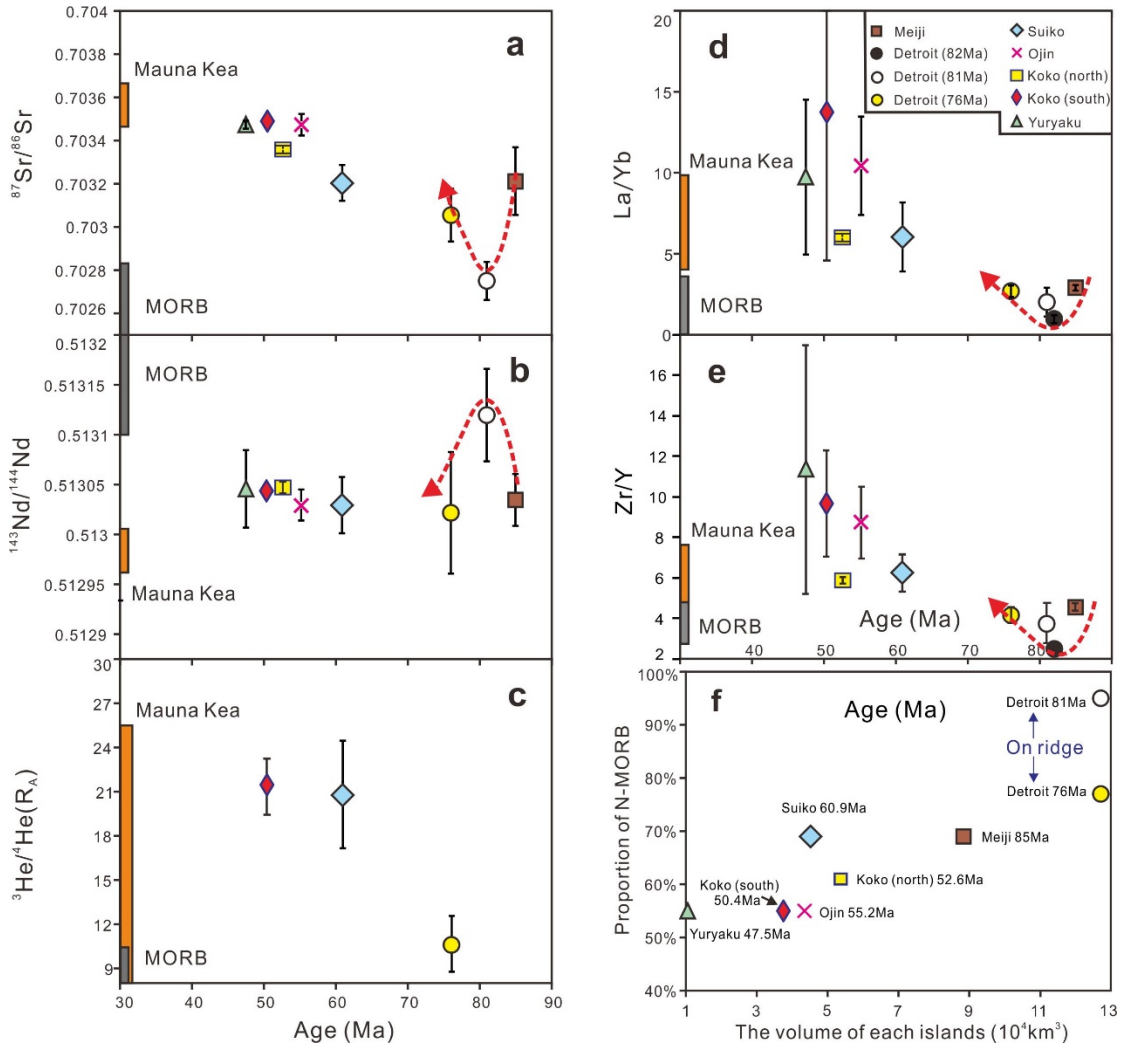

Figure 3. **Changes of the geochemical characteristics of basalts from the Hawaiian-Emperor chain with age**. **a.** $^{87}Sr/^{86}Sr$; **b**. $^{143}Nd/^{144}Nd$; **c.** $^{3}He/^{4}He$; **d.** La/Yb; **e.** Zr/Y. **f.** The volumes of the Emperor Seamounts are positively correlated with proportions of MORB components. The volumes of Meiji and Detroit are very large, comparable to oceanic plateaus with large proportions of MORB components, supporting plume-ridge interactions. The declining MORB components southward may best be explained by the southward migration of the Hawaiian plume and increasing age (and thus thickness) of the oceanic crust. Data are listed in the Supplementary materials.

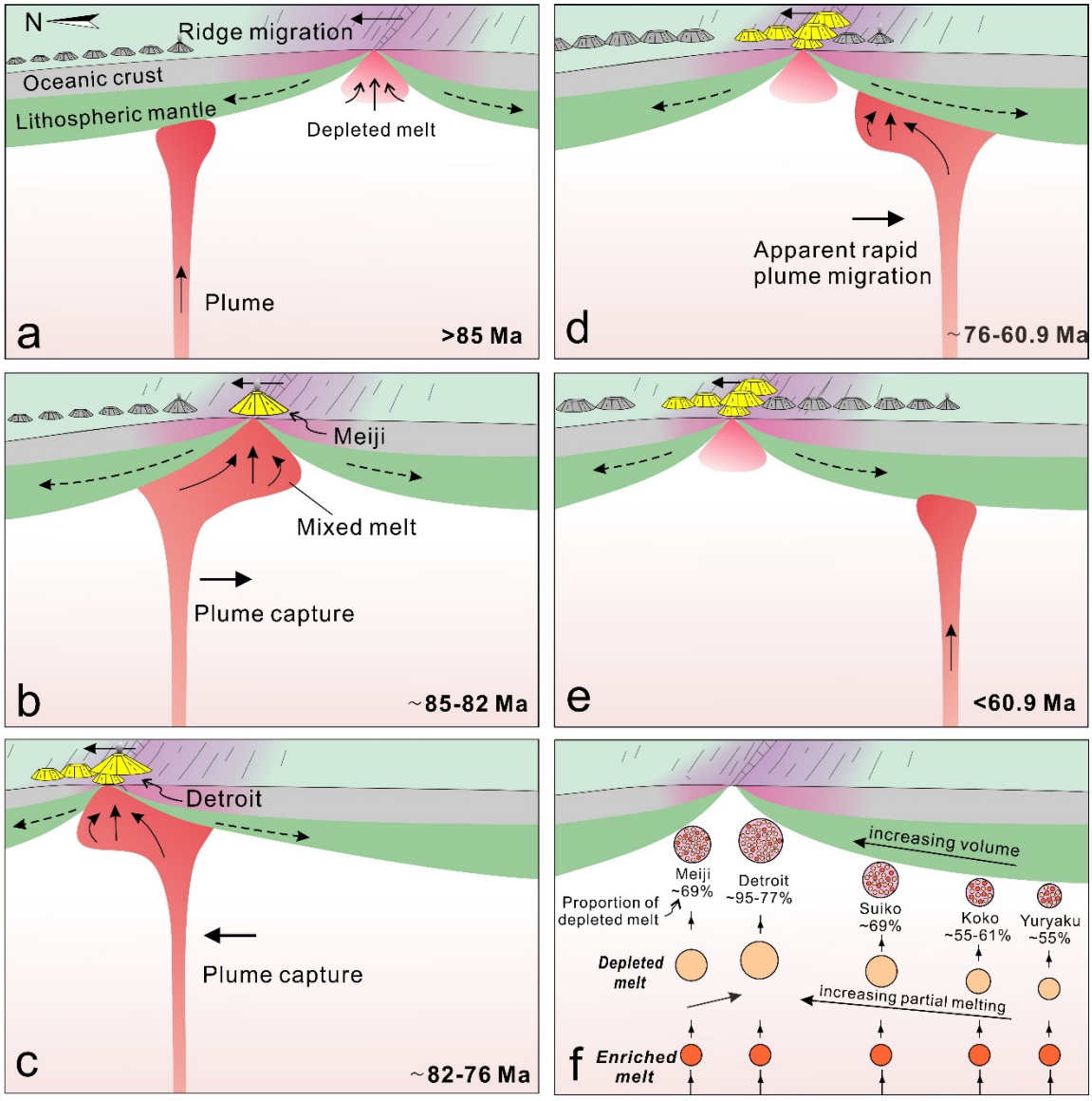

Figure 4. **a-f. Cartoon showing ridge-plume interactions when the northward migrating spreading ridge passed the originally stationary Hawaiian mantle plume. a.** The Hawaiian plume was originally located to the north of the spreading ridge between Pacific and Izanagi plates. **b.** Plume is attracted southward, intensified with increasing proportion of MORB component as the spreading ridge approaches (Meiji), because of decreasing thickness of the overriding plate. **c, d.** Plume is channeled to the ridge, and is further intensified, with more MORB component as the ridge moves further north, carrying the plume with it. Meanwhile migration of the ridge is probably slowed down due to plume-ridge interaction. **e.** As the ridge moves further to the north, it lost

contact with the plume, such that the magmatism from the plume migrates rapidly southwards, leading to very low volumes at the surface during the transit. **f.** Cartoon illustrating the volume and proportions of MORB and plume components of the Emperor seamounts. The mixing simulation data are listed in the Supplementary materials

SUPPLEMENTARY INFORMATION

Plume-ridge interaction induced migration of the Hawaiian-Emperor plume

Wei-dong Sun[1-3]*, Charles H. Langmuir[4]*, Neil M. Ribe[5], Li-peng Zhang[1,3], Sai-jun Sun[1,3], He Li[1,2], Cong-ying Li[1,2], Wei-ming Fan[3,6], Paul J. Tackley[7] and Patrick Sanan[7]

[1] Center of Deep Sea Research, Center of Ocean Mega Science, Institute of Oceanology, Chinese Academy of Sciences, Qingdao 266071, China

[2] Laboratory for Marine Mineral Resources, Pilot National Laboratory for Marine Science and Technology (Qingdao), Qingdao 266237, China

[3] University of the Chinese Academy of Sciences, Beijing 100049, China

[4] Department of Earth and Planetary Sciences, Harvard University, Cambridge, USA.

[5] Univ Paris 11, CNRS, Lab FAST, F-91405 Orsay, France

[6] CAS Center for Excellence in Tibetan Plateau Earth Sciences, Chinese Academy of Sciences, Beijing 100101, China

[7] Institute of Geophysics, Department of Earth Sciences, ETH Zurich, Sonneggstrasse 5, 8092 Zűrich, Switzerland*

*Corresponding authors: Wei-dong Sun; Charles H. Langmuir.

Email: weidongsun@qdio.ac.cn; langmuir@eps.harvard.edu

This PDF file includes:

Supplementary text

SUPPLEMENTARY INFORMATION

Figures S1 to S7

Tables S1 to S2

SI References

Other supplementary materials for this manuscript include the following:

Datasets S1 to S2

SUPPLEMENTARY INFORMATION

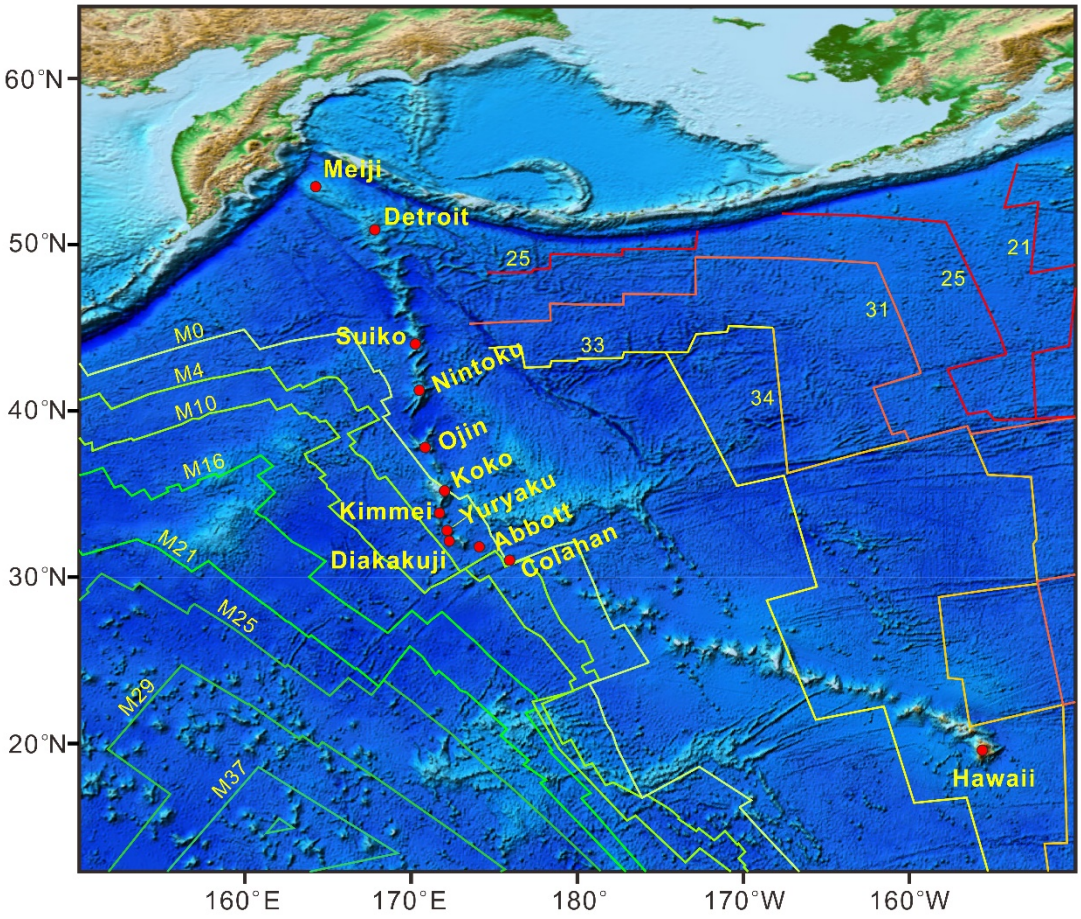

Figure S1 Map showing Hawaiian-Emperor chains and magnetic anomalies.

1. Volume calculation

The volumes of the Emperor seamounts have been calculated in two different ways using ArcGIS: First, along track volume of every 0.5 degrees; Second, volumes of individual seamounts.

ArcGIS is a GIS (Geographic Information System) software, developed by ESRI (Environmental Systems Research Institute, US). It has powerful spatial analysis ability. We use the 3D Analyst module in Arc Toolbox to calculate volume based on bathymetry data. Bathymetry data, a 15 arc-second grid, is from the General Bathymetric Chart of the Oceans, GEBCO (https://www.gebco.net/), which is the latest global bathymetric product. First, we define the projected coordinate system of the bathymetric data as

SUPPLEMENTARY INFORMATION

Robinson. Then, each slice or seamount is clipped out from the projected bathymetry data using Raster Processing module in Arc Toolbox. Each slice or seamount chooses an altitude as the reference plane based on the height variations of seabed around the slice or seamount, and the volume above the plane is calculated. For the along track volume calculation, the seamount chain was first sliced every 0.5 degrees (Figure S2). The volume of each slice has been calculated, and the result is listed in Table S1. The Hawaiian-Emperor seamounts are either as isolated or as clustered volcanic shields. We divided the chain into individual seamounts based upon the change of the seamount elevation and the relationship with adjacent seamounts (Figure S3). The volume has been calculated for each seamount. In this study, we mainly focus on the volume of eight seamounts, namely Meiji, Detroit, Suiko, Ojin, Koko, Kimmei, Yuryaku and Daikakuji, the calculated results are summarized in Table S2.

SUPPLEMENTARY INFORMATION

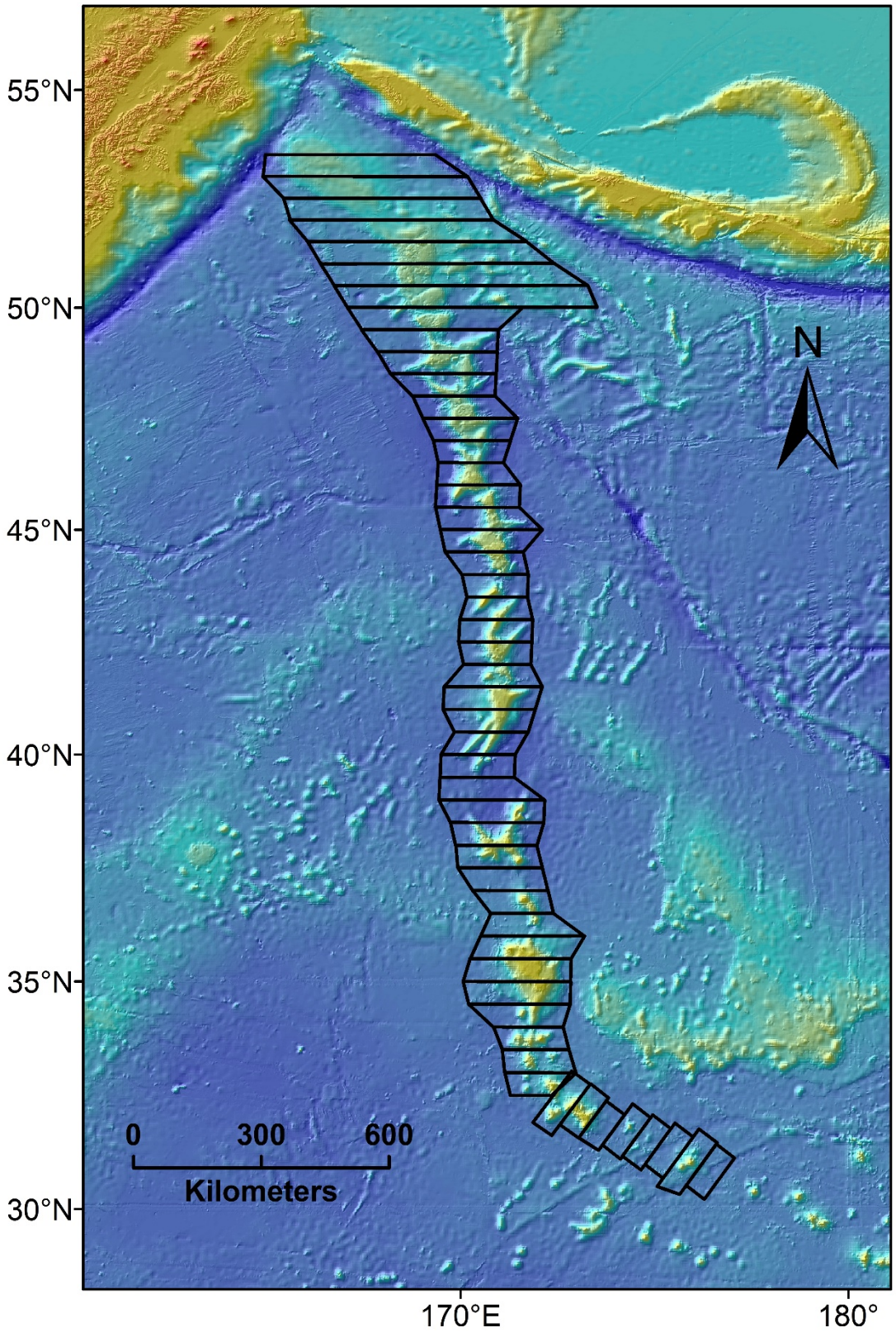

Figure S2 Along track slices used for volume calculation.

SUPPLEMENTARY INFORMATION

Table S1 Along Emperor track volumes from Meiji for every 0.5 degrees

No.	Reference plane (m)	Volume ($\times 10^3$ km^3)	No.	Reference plane (m)	Volume ($\times 10^3$ km^3)
1	-5500	27.0	26	-6100	16.7
2	-5500	28.6	27	-6200	10.5
3	-5100	18.4	28	-6250	4.63
4	-5200	26.2	29	-6100	1.56
5	-5200	27.6	30	-6200	8.66
6	-5200	27.3	31	-6000	16.1
7	-5200	24.8	32	-6000	18.2
8	-5600	15.1	33	-5800	4.60
9	-6000	17.7	34	-5400	8.04
10	-6200	22.7	35	-5200	4.60
11	-6200	14.5	36	-5400	21.2
12	-6200	13.8	37	-5400	28.5
13	-6400	19.3	38	-5400	19.8
14	-6400	11.8	39	-5600	9.24
15	-6400	14.6	40	-5800	11.9
16	-6400	17.7	41	-5800	10.9
17	-6000	10.7	42	-5600	8.88
18	-6400	20.2	43	-5600	11.8
19	-6300	12.9	44	-5500	11.1
20	-5800	6.18	45	-5500	1.72
21	-5900	11.2	46	-5400	1.59
22	-6000	12.4	47	-5500	2.35
23	-5600	11.7	48	-5500	1.44
24	-5800	11.1	49	-5500	7.31
25	-5700	18.3	50	-5500	1.27

SUPPLEMENTARY INFORMATION

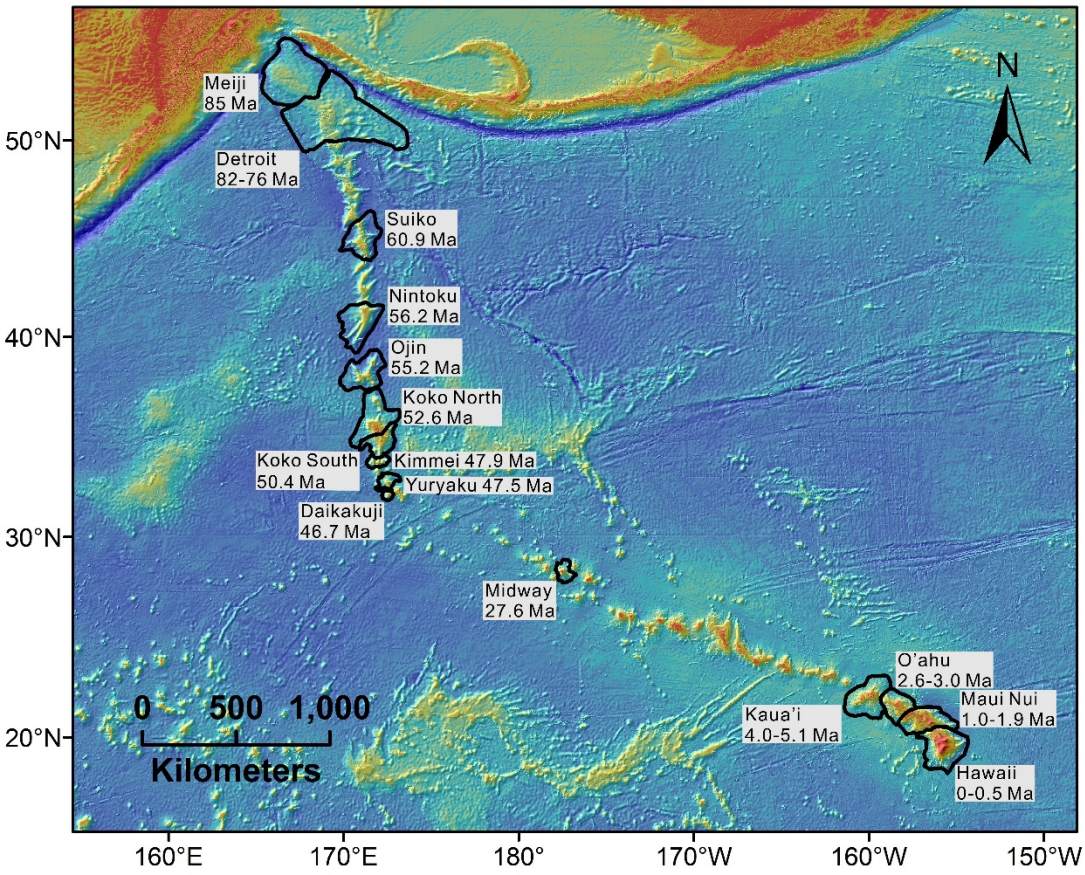

Figure S3 Areas of seamounts used for volume calculation.

SUPPLEMENTARY INFORMATION

Table S2 The individual seamount volumes of the Hawaiian-Emperor chain

Seamount	Reference plane (m)	Area ($\times 10^3$ km^2)	Volume ($\times 10^3$ km^3)	Age (Ma)	Analytical method	Stage	Age reference
Meiji	-5500	70.8	88.1	85		Shield	1,2
Detroit	-5200	129.6	126.6	82-76	^{40}Ar/^{39}Ar	Shield and postshield	1,2,3,4
Suiko	-6000	25.7	45.0	60.9	^{40}Ar/^{39}Ar	Shield and postshield	5
Nintoku	-5700	26.7	44.7	56.2	^{40}Ar/^{39}Ar	Postshield	2
Ojin	-6000	27.0	43.6	55.2	^{40}Ar/^{39}Ar	Shield and postshield	2
Koko North	-5400	36.7	54.0	52.6	^{40}Ar/^{39}Ar	Shield	5
Koko South	-5400	17.4	38.0	50.4	^{40}Ar/^{39}Ar	Postshield	5
Kimmei	-5800	5.77	10.8	47.9	^{40}Ar/^{39}Ar	Postshield	5
Yuryaku	-5400	7.18	9.74	47.5	^{40}Ar/^{39}Ar	Late shield	6
Daikakuji	-5500	2.34	3.80	46.7	^{40}Ar/^{39}Ar	Shield	5
Midway	-5500	8.0	13.7	27.6	^{40}Ar/^{39}Ar	Shield	6
Kaua'i	-4800	35.9	51.6	4.0-5.1	K-Ar	Shield	7,8
O'ahu	-4800	19.4	44.6	2.6-3.0	K-Ar	Shield	7,9
Maui Nui	-5600	29.0	103.6	1.0-1.9	K-Ar	Shield	7,10
Hawaii	-5600	42.8	134.3	0-0.5	K-Ar	Shield	7,10

Note：The ^{40}Ar/^{39}Ar age is measured using step heating technique.

2. Numerical modeling

Plume-ridge interaction numerical modeling is conducted using the code StagYY (11). This code employs a finite-volume multigrid method to solve for inertia-free flow in a fluid with variable viscosity.

The model domain is a rectangular box 400 km deep (the z-direction), 2400 km long (the x-direction), and 800 km wide (the y-direction). It is divided into 288 × 96 × 48 elementary volumes with horizontal dimensions $dx = dy = 8.33$ km and variable vertical dimension (the grid is refined near the top of the box).

SUPPLEMENTARY INFORMATION

The box is filled with a Newtonian fluid whose viscosity □ depends on temperature T, pressure p and equilibrium melt fraction F as

$$\eta = \eta_0 \exp\left(\frac{E+pV}{RT} - \frac{E}{RT_0}\right)\left[1 + \Delta\eta \tanh\left(\frac{F}{\Delta F}\right)\right] \qquad (\text{I})$$

In (I), $\eta_0 = 10^{19}$ Pa s is the reference viscosity at temperature T_0 = 1600 K and zero pressure, E = 3× 10^5 J/mole is the activation energy and V = 3× 10^{-6} m^3/mole is the activation volume. The quantity 1 + □□ = 10 is the maximum factor by which melting increases the viscosity, and □F = 0.05.

Flow in the model box comprises a passive (ridge) and an active (plume) component. The ridge component is driven by an imposed surface velocity

$$u = U \tanh\left(\frac{x - x_{\text{ridge}}(t)}{d}\right) \qquad (\text{II})$$

where U is the half-spreading rate, d = 25 km is the characteristic width of the ridge, and $x_{\text{ridge}}(t)$ is the time-dependent position of the ridge. The velocity of ridge migration is assumed to be parallel to the spreading velocity, and both are in the x-direction. The ridge migration speed is

$$u_{\text{ridge}}(t) = \frac{U_m}{2}\left[1 + \tanh\left(\frac{t - t_1}{t_2}\right)\right] \qquad (\text{III})$$

where t_1 = 40 Ma, t_2 = 10 Ma, and U_m is the ridge migration speed in the limit $t \gg t_1$. Eqn. (III) implies that the ridge is nearly stationary for 40 Ma (to give the developing plume time to mature), and then gradually accelerates during ≈ 10 Ma to its final constant speed U_m. The corresponding ridge position is

$$x_{\text{ridge}}(t) = x_{\text{ridge}}(0) + \int_0^t u_{\text{ridge}}(T)\,\mathrm{d}T \qquad (\text{IV})$$

where $x_{\text{ridge}}(0)$ is the initial position.

The plume component of the flow is generated by a fixed (non-migrating) temperature boundary condition on the lower surface of the box of the form

$$T = T_0 + \Delta T \exp\left(-\frac{r^2}{a^2}\right) \qquad (\text{V})$$

where ΔT is the excess temperature of the plume, a km is its radius, and $r^2 = \left(x - x_{\text{plume}}\right)^2 + y^2$ where x_{plume} is the x-coordinate of the center of the Gaussian temperature anomaly. Because the flow is symmetric about the vertical plane y = 0, the

model domain is limited to $y \geq 0$.

Melting in the model domain is calculated using the parameterization of McKenzie and Bickle (1988) (12), which delivers the melt fraction $F(T, p)$ as a function of temperature and pressure. The local rate of melt production is then

$$\Gamma = \frac{DF}{Dt} \qquad \text{(VI)}$$

where D/Dt is the convective time derivative that follows the motion of a material particle. The units of Γ are s^{-1}, or m^3 of melt per m^3 of source material per second. Finally, the total rate of melt production beneath a point (x, y) at the surface $z = 0$ is

$$q(x,y) = \int_{-d}^{0} \max(0,\Gamma)dz \qquad \text{(VII)}$$

where d = 400 km. The 'max' in the integrand means that q accounts only for melting ($\Gamma > 0$), and does not include any negative contributions due to freezing ($\Gamma < 0$). This is because melt is assumed to be extracted before it refreezes. The quantity $q(x, y)$ is equal to the flux of melt at (x, y) only if all melt is extracted vertically, which is not in general the case. However, the spatial resolution of our large-scale numerical models is not adequate for calculating reliable melt trajectories. We therefore use q as a measure of the amount of melt produced beneath a given point.

To define a reference plume-ridge interaction model we use a number of geophysical constraints. First, the rates of northward drift of the Pacific and Izanagi plates at the time of interaction of the ridge with the plume were ≈ 10 cm/yr and 20 cm/yr, respectively (13). Those values imply U = 5 cm/yr and U_m = 15 cm/yr. Second, the duration of eruption of the ridge-influenced seamounts Detroit and Meiji was ≈ 9 Ma (1-4). Third, the length of the Meiji volcanic edifice along the ridge was ≈ 300 km. Finally, the total volume of Detroit and Meiji before erosion was ≈ 6.5×10^5 km^3.

To satisfy the constraint on the volume of Detroit and Meiji, we adjusted the strength of the plume by varying its radius a while the excess temperature □T = 225 K was held fixed. The volumetric melt flux to the ridge at each time step was calculated by collecting the melt formed within 50 km to either side of the ridge and over an along-strike distance of 300 km. The total volume of erupted melt was then calculated by

integrating the volumetric flux with respect to time over 9 Ma starting when plume-ridge interaction was just beginning (between the times of Figure S4a and S4b). The iterative process just described yields a = 62 km for a total melt volume 6.7×10^5 km^3. The buoyancy flux of the plume varies by about 33% as the ridge moves over it, but the maximum value is 1500 kg/s. This can be compared with the estimate of ≈ 2800 kg/s for the present-day Hawaiian plume (14).

It is also possible to estimate how much of the total melt flux q is derived from the plume source as opposed to the MORB source. To do this, we assumed that melting occurring at a temperature $T > 1.01T_0$ □ 1616 K involves the plume source, whereas melting at lower temperatures involves the MORB source. We then used (Ⅶ) to calculate separately the flux q_1 from the plume source and the flux q_2 from the MORB source. Figure S5 shows the results for the reference model at the time corresponding to Figure S4b. The contours of q_1 are roughly concentric due to the geometry of the plume, whereas the more linear contours of q_2 testify to passive upwelling beneath the ridge. The domains of nonzero q_1 and q_2 overlap, indicating that melts from the plume and MORB sources can be generated at different depths beneath the same point on the surface. This overlap of melting domains may provide an efficient mechanism for mixing of melts from the plume and MORB sources.

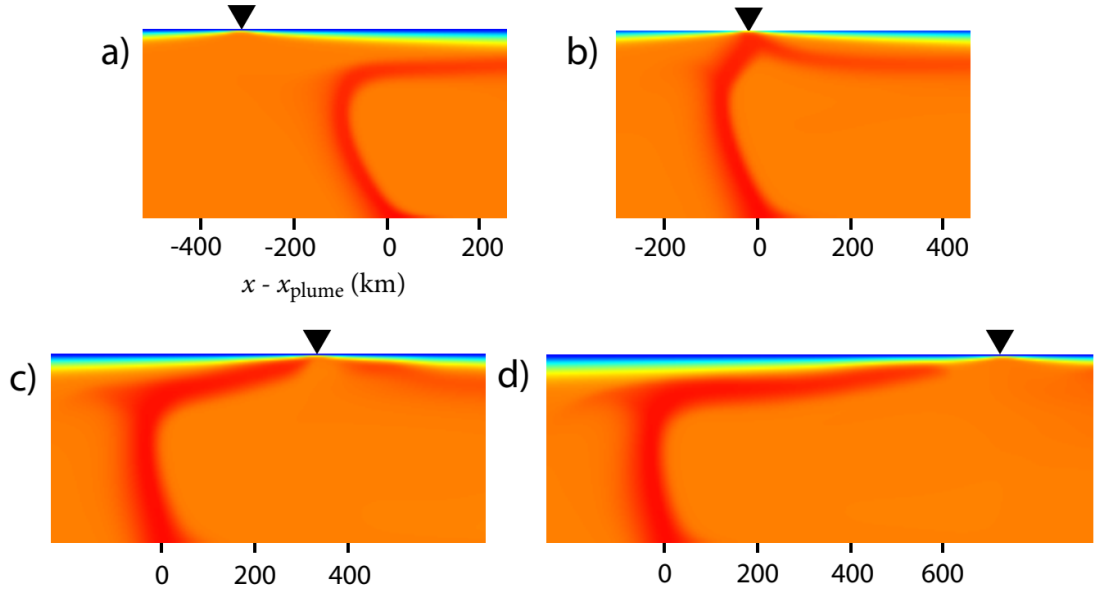

Figure S4 Temperature fields in the vertical symmetry plane y = 0 of the reference

model at four different stages of plume-ridge interaction. The ridge moves from left to right relative to the plume, and its position is indicated by inverted triangles. The plume is generated by a fixed Gaussian hot patch with radius 62 km and maximum excess temperature 225 K. The temperature in the images ranges from 273 K (blue) to 1825 K (red), and the temperature of the mantle away from the plume is 1600 K (orange).

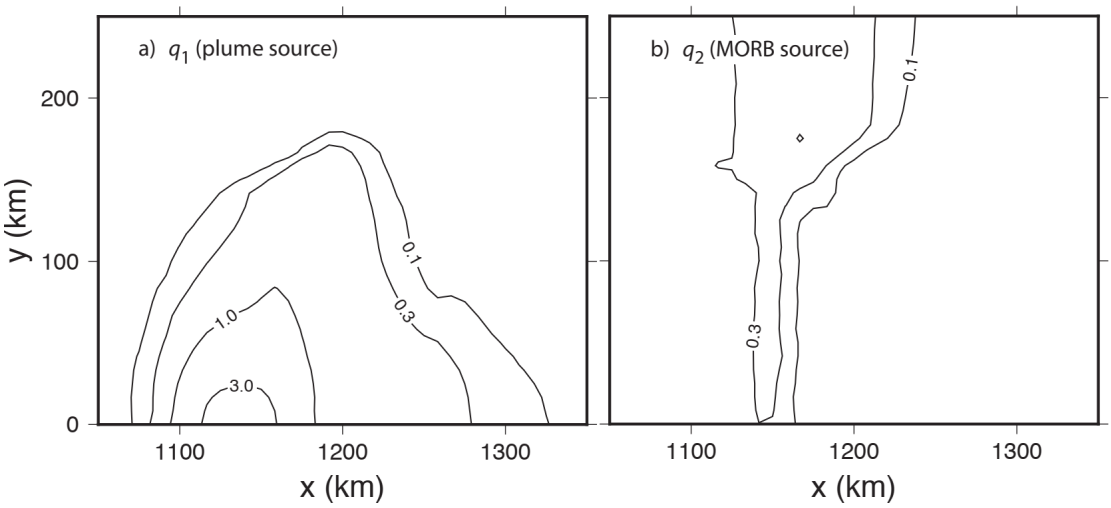

Figure S5 Melt fluxes $q_1(x, y)$ and $q_2(x, y)$ (cm/yr) derived from the plume and MORB sources, respectively, for the reference model at the time corresponding to Figure S4b.

3. Two-component mixing

The two-component mixing model is widely used in geochemistry. The mixing can be described using the following Equation:

$AX+BXY+CY+D=0$ (Ⅷ)

Where:

$A=a_2b_1y_2-a_1b_2y_1$;

$B=a_1b_2-a_2b_1$;

$C=a_2b_1x_1-a_1b_2x_2$;

$D=a_1b_2x_2y_1-a_2b_1x_1y_2$;

$P=a_1b_2/a_2b_1=P_1/P_2$.

The a_1 and a_2 are the y variable denominator isotope content of component 1 and component 2 respectively. The b_1 and b_2y are the x variable denominator isotope

SUPPLEMENTARY INFORMATION

content of component 1 and component 2 respectively. P is the curvature value of simulation curve. X and Y can be isotopic ratio, element ratio or element content.

N-MORB and OIB are used as the component 1 and 2. The compositions are: $(^{87}Sr/^{86}Sr)_{N\text{-}MORB}$=0.70264; $(^{143}Nd/^{144}Nd)_{N\text{-}MORB}$=0.51313; $(La/Yb)_{N\text{-}MORB}$=0.82; $(^{87}Sr/^{86}Sr)_{OIB}$=0.7045; $(^{143}Nd/^{144}Nd)_{OIB}$=0.51263; $(La/Yb)_{OIB}$=17.1; The above component data comes from previous studies (15-17).

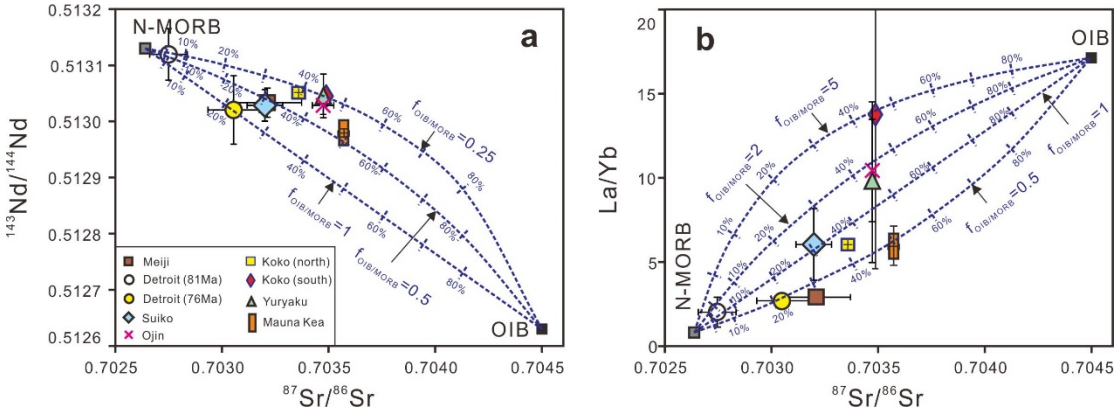

Figure S6 Diagrams of $^{87}Sr/^{86}Sr$ versus $^{143}Nd/^{144}Nd$ (a) and La/Yb (b), indicating that the Emperor Seamount chain formed by different proportions of mixing between OIB and N-MORB. The data come from supplementary Datasets S1 and S2.

SUPPLEMENTARY INFORMATION

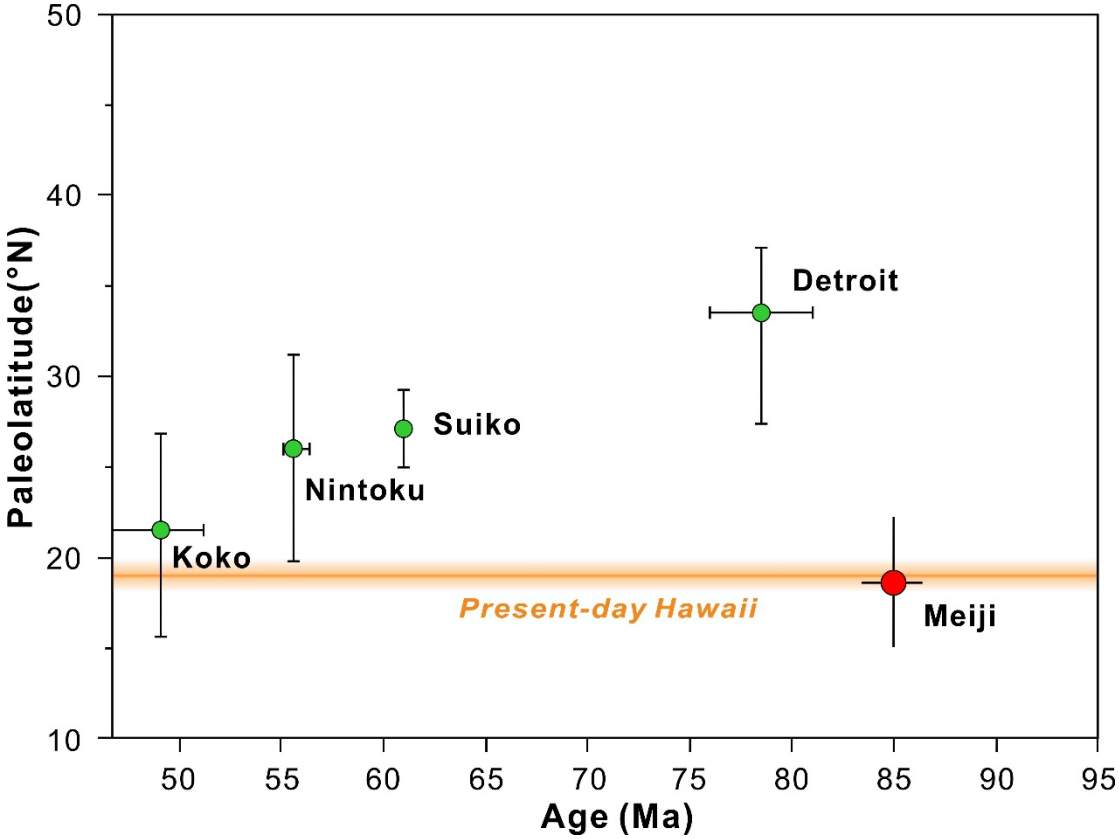

Figure S7 The paleolatitude of the Emperor Seamount chain. Paleolatitude data are from previous studies (18-20).

4. Geochemical data of Hawaiian Chain and East Pacific Rise

The results of geochemical data and standard deviation from Hawaiian Chain are listed in Dataset S2. Geochemical data of East Pacific Rise and volumes vs. mixing ratios of individual islands are included in the Dataset S2. The above geochemical data are from previous studies (2, 4, 21-29).

References

1. Keller RA, Fisk MR, White WM. Isotopic evidence for Late Cretaceous plume–ridge interaction at the Hawaiian hotspot. *Nature* **405**, 673-676 (2000).
2. Regelous M, Hofmann AW, Abouchami W, Galer SJG. Geochemistry of lavas from the Emperor Seamounts, and the geochemical evolution of Hawaiian magmatism from 85 to 42 Ma. *J. Petrol.* **44**, 113-140 (2003).
3. Duncan RA, Keller RA. Radiometric ages for basement rocks from the Emperor Seamounts,

SUPPLEMENTARY INFORMATION

ODP Leg 197. *Geochem. Geophys. Geosyst.* **5** (2004).

4. Huang S, Regelous M, Thordarson T, Frey F. Petrogenesis of lavas from Detroit Seamount: Geochemical differences between Emperor Chain and Hawaiian volcanoes. *Geochem. Geophys. Geosyst.* **6** (2005).
5. Sharp WD, Clague DA. 50-Ma initiation of Hawaiian-Emperor bend records major change in Pacific plate motion. *Science* **313**, 1281-1284 (2006).
6. O'Connor JM, Steinberger B, Regelous M, Koppers AA, Wijbrans JR, Haase KM, et al. Constraints on past plate and mantle motion from new ages for the Hawaiian-Emperor Seamount Chain. *Geochem. Geophys. Geosyst.* **14**, 4564-4584 (2013).
7. Robinson JE, Eakins BW. Calculated volumes of individual shield volcanoes at the young end of the Hawaiian Ridge. *Journal of volcanology and geothermal research* **151**, 309-317 (2006).
8. Garcia MO, Frey FA, Grooms DG. Petrology of volcanic rocks from Kaula Island, Hawaii. *Contributions to Mineralogy and Petrology* **94**, 461-471 (1986).
9. Guillou H, Sinton J, Laj C, Kissel C, Szeremeta N. New K–Ar ages of shield lavas from Waianae Volcano, Oahu, Hawaiian Archipelago. *Journal of Volcanology and Geothermal Researc* 2000, **96**, 229-242 (2000).
10. Clague DA, Dalrymple GB. The Hawaiian-Emperor volcanic chain. part I. Geologic evolution. *Volcanism in Hawaii*, **1**: 5-54 (1987).
11. Tackley PJ. Modelling compressible mantle convection with large viscosity contrasts in a three-dimensional spherical shell using the yin-yang grid. *Physics of the Earth and Planetary Interiors* **171**, 7-18 (2008).
12. McKenzie D, Bickle MJ. The volume and composition of melt generated by extension of the lithosphere. *J. Petrol.* **29**, 625-679 (1988).
13. Maruyama S, Isozaki Y, Kimura G, Terabayashi M. Paleogeographic maps of the Japanese Islands: Plate tectonic synthesis from 750 Ma to the present. *Isl. Arc.* **6**, 121-142 (1997).
14. Ribe NM, Christensen UR. The dynamical origin of Hawaiian volcanism. *Earth and Planetary Science Letters* **171**, 517-531 (1999).
15. Ito E, White WM, Göpel C. The O, Sr, Nd and Pb isotope geochemistry of MORB. *Chemical Geology* **62**, 157-176 (1987).

SUPPLEMENTARY INFORMATION

16. Sun SS, McDonough WS. Chemical and isotopic systematics of oceanic basalts: implications for mantle composition and processes. *Geological Society, London, Special Publications* **42**, 313-345 (1989).

17. Zindler A, Hart S. Chemical geodynamics. *Annual review of earth and planetary sciences* **14**, 493-571 (1986).

18. Tarduno JA, Duncan RA, Scholl DW, Cottrell RD, Steinberger B, Thordarson T, Kerr BC, Neal CR, Frey FA, Torii M, Carvallo C. The Emperor Seamounts: Southward motion of the Hawaiian hotspot plume in earth's mantle. *Science* **301**, 1064-1069 (2003).

19. Marshall M. Magnetic-properties of some DSDP basalts from North Pacific and inferences for Pacific plate tectonics. *Journal of Geophysical Research* **83**, 289-308 (1978).

20. Sager WW, Lamarche AJ, Kopp C. Paleomagnetic modeling of seamounts near the Hawaiian-Emperor bend. *Tectonophysics* **405**, 121-140 (2005).

21. Blichert-Toft J, Weis D, Maerschalk C, Agranier A, Albarède F. Hawaiian hot spot dynamics as inferred from the Hf and Pb isotope evolution of Mauna Kea volcano. *Geochem. Geophys. Geosyst.* **4** (2003).

22. Broadley MW, Sumino H, Graham DW, Burgess R, Ballentine CJ. Recycled Components in Mantle Plumes Deduced From Variations in Halogens (Cl, Br, and I), Trace Elements, and 3He/4He Along the Hawaiian-Emperor Seamount Chain. *Geochem. Geophys. Geosyst.* **20**, 277-294 (2019).

23. Huang S, Frey FA. Trace element abundances of Mauna Kea basalt from phase 2 of the Hawaii Scientific Drilling Project: Petrogenetic implications of correlations with major element content and isotopic ratios. *Geochem. Geophys. Geosyst.* **4**, doi:10.1029/2002gc000322 (2003)

24. Keller RA, Graham DW, Farley KA, Duncan RA, Lupton E. Cretaceous-to-recent record of elevated He-3/He-4 along the Hawaiian-Emperor volcanic chain. *Geochem. Geophys. Geosyst.* **5** (2004).

25. Kurz MD, Curtice J, Lott III DE, Solow A. Rapid helium isotopic variability in Mauna Kea shield lavas from the Hawaiian Scientific Drilling Project. *Geochem. Geophys. Geosyst.* **5** (2004).

26. Niu YL, Collerson KD, Batiza R, Wendt JI, Regelous M. Origin of enriched-type mid-ocean

SUPPLEMENTARY INFORMATION

ridge basalt at ridges far from mantle plumes: The East Pacific Rise at 11 degrees 20 ' N. *Journal of Geophysical Research-Solid Earth* **104**, 7067-7087 (1999).

27. Regelous M, Niu YL, Wendt JI, Batiza R, Greig A, Collerson KD. Variations in the geochemistry of magmatism on the East Pacific Rise at 10 degrees 30 ' N since 800 ka. *Earth and Planetary Science Letters* **168**, 45-63 (1999).

28. Rhodes JM, Vollinger MJ. Composition of basaltic lavas sampled by phase-2 of the Hawaii Scientific Drilling Project: Geochemical stratigraphy and magma types. *Geochem. Geophys. Geosyst.* **5** (2004).

29. Silva IGN, Weis D, Scoates JS. Isotopic systematics of the early Mauna Kea shield phase and insight into the deep mantle beneath the Pacific Ocean. *Geochem. Geophys. Geosyst.* **14**, 659-676 (2013).